# Seismic wave propagation around subsurface igneous sill complexes

*Sanford, O. G.* [1]*, Schofield, N.* [2]*, Hobbs, R. W.* [1]*, Brown, R. J.* [1]

[1] Durham University, Department of Earth Sciences, Durham, DH1 3LE, UK
[2] University of Aberdeen, Department of Geology & Petroleum Geology, Aberdeen, AB24 3UE, UK

## Abstract

Imaging both within and beneath subsurface igneous sill complexes is a seismic exploration challenge. A significant aspect of this challenge is due to a lack of understanding of the interaction between the heterogeneous geological structures and the seismic wavefield which includes the seismic response to sub-resolution 'thin' sills. This study aims to provide some insight into the effect of subsurface sills have on the observed seismic wavefield. This is achieved through high resolution full-waveform elastic seismic modelling, using a realistic geological model developed from interpreted seismic data and statistics of sills from wireline logs. We find that little energy penetrates through the sill complex to a target reflector below the sill complex, which is consistent with real-world observations. This is due to a number of factors, including energy lost to strong internal multiples (stratigraphic filtering), converted modes and leaky guided waves within the sills. These processes remove energy from the primary transmitted wavefront, contributing to degraded seismic imaging. Whilst these are all fundamental physical limitations that cannot be overcome, further work should focus on the processing of seismic data to ensure that these aspects of the seismic wave-field around sill complexes are optimally treated within processing workflows.

Keywords: seismic; wave propagation; sills; intrusions

## 1. Introduction

Subsurface intrusive sill complexes are often considered to be well-imaged using seismic reflection techniques. This is due to the relative internal homogeneity and strong impedance contrast of a high-velocity, high density sill intrusion within a lower velocity, lower density sedimentary host rock, particularly when compared to the challenges associated with extrusive basalt sequences (Martini & Bean 2002, Maresh *et al.* 2006, Gallagher & Dromgoole 2007). Hydrocarbon exploration has increasingly focussed on sedimentary basins that contain igneous sill intrusions. Extensive 3D seismic datasets, supplemented by field observations, have helped improve our understanding of subsurface igneous sill complexes, which represent a major form of magma transport within the crust (Smallwood & Maresh 2002, Thomson & Hutton 2004, Archer *et al.* 2005, Cartright and Hansen 2006, Muirhead *et al.* 2012, Wright *et al.* 2012, Schofield *et al.* 2012, Schofield *et al.* 2015, Magee *et al.* 2016, Airoldi *et al.* 2016). Recent research has shown that up to 90% of the sills penetrated by boreholes are 'sub-resolution', where they are below the limits of vertical seismic resolution and are often missed during seismic interpretation (Mark *et al.* 2017, Schofield *et al.* 2015). Furthermore, whilst mafic sills typically have a high-velocity and density, due to their Fe- and Mg-rich mineralogy, silicic sills commonly have a lower velocity and density, resulting in a lower impedance contrast with sedimentary rocks and a weaker seismic reflection (Mark *et al.* 2017). During processing, strong internal multiples may contaminate the final migrated image, giving rise to the appearance of sills that are not actually present (Hardy *et al.* 2008), Vertical and sub-vertical igneous dykes are also missed during conventional imaging. A well-known example of poor sill imaging comes from the Rockall Trough, where based upon seismic interpretation, well 164/07-1 was targeting a series of sub-basalt reflections interpreted as interbedded

sandstones and shales, however upon drilling the reflectors where actually found to consist of a series of sill intrusions ranging in thickness from 1.5 m to 152 m that where parallel to the regional stratigraphy (Archer *et al.* 2005).

Sill complexes can have a close association with hydrocarbon sources and reservoirs (Rateau *et al. 2013*), and reliable seismic imaging is critical for the correct interpretation. There have been limited studies into the seismic response of sills based upon seismic modelling. 1D convolution modelling using simple planar geometries of sills (Magee *et al.* 2015) can give indications of the tuning thickness of sills but is of limited use when generating a realistic seismic response. Point spread function convolution modelling can generate data equivalent to pre-stack depth migration (Lecomte *et al.* 2016) and provide a more realistic and computationally fast seismic response to an input model. These studies often use scaled field outcrop models from photogrammetry (Eide *et al.* 2017, Rabbel *et al.* 2018), indicating that sub-resolution thin sills may be detected on seismic data in the absence of noise. However, these studies are focussed on seismic interpretation, rather than the underlying interaction between the seismic wavefield and the complex intrusion network, and neglect the loss of signal throughout a sequence. Hardy et al. (2008) use acoustic full-wavefield seismic modelling and geologically constrained model of a sill complex to show the challenges of seismic processing around intrusion networks. They show that migration artefacts in the final image, which are caused by internal multiples, may give the appearance of sills that are not present and can result in false interpretations of the subsurface structure.

This study seeks to address the knowledge gap of the underlying interaction between the seismic wavefield and the complex intrusion network, by using elastic full-waveform modelling to identify the wave propagation processes around subsurface sill complexes to

better understand the interaction of the wavefield with the sills and how this contributes to reduced sill and sub-sill imaging.

## 2. Methods

To generate a realistic geological model of a sill complex, both the seismically resolvable 'thick' sills and sub-resolution 'thin' sills must be considered, as the sills imaged on seismic datasets may only represent ~10% of the total intruded volume (Mark *et al.* 2017, Schofield *et al.* 2015). We use an example based on morphology of an interpreted sill complex from the Paleogene Faroe-Shetland Sill Complex within the Faroe-Shetland basin, in the North Atlantic (see Figure 11 of Schofield et al. 2015). This is a network of interconnected 'thick sills', where it is known from well 205/10-2B that large volumes of thin sills are located around the network.

Based upon field evidence of sill networks from the Henry Mountains, Utah (Mark *et al.* 2019), the proportion of thin sills is greatest in the vicinity of large intrusions and reduces away from the thick sill complex. It is not possible to apply sub-resolution 'thin' sills in a deterministic sense (as with the 'thick' sills, which are taken directly from interpreted seismic data), so a stochastic model is developed instead. Other authors use direct field analogues to model the 'thin' sills (Eide *et al.* 2017, Rabbel *et al.* 2018), but the methodology we apply is based upon 'random media theory', which is an effective method to model stochastic heterogeneity within the Earth's crust (Goff *et al.* 1994, Levander *et al.* 1994, Goff & Levander 1996). By combining a large-scale velocity structure (deterministic) and smaller-scale heterogeneities (stochastic), a range of geological scales may be modelled (Larkin *et al.* 1996). Following a similar approach, a series of 'thin' sills are mapped onto the 'thick' sill network that follow the underlying

regional stratigraphy and reduce in number away from the sill complex, as observed in the field (Mark *et al.* 2019).

Figure 1 shows the P-wave velocity model. A simple syncline with a compaction gradient (approximately 0.5 $s^{-1}$) lies under a flat seabed at 500 m depth. This represents the background sedimentary succession but lacks any internal impedance contrasts so that it does not generate any reflectivity that would confuse interpretation of the reflectivity from the igneous intrusions. Onto this background model is added the deterministic sill complex taken from an interpretation of a section of the Faroe-Shetland Sill Complex by Schofield et al. (2015), and a stochastic range of thin sills morphed to follow the contours of the background sedimentary model. The P-wave velocity of the sills is set at a single value of 5.75 km $s^{-1}$, the average sill velocity from well 205/10-2B (Mark *et al.* 2017). Below the sill complex is a high impendance sub-sill target reflector (P-wave velocity=6 km $s^{-1}$), used to test the degradation of the wavefield below sill complexes. An S-wave and density model are generated based upon an empirical relation with the P-wave velocity derived from Brocher, 2005. No intrinsic attenuation is included within the model, so any signal loss is solely from wave propagation and scattering effects due to the sill complex.

Full seismic wavefield modelling following a 2-D elastic finite-difference approach is undertaken using *SOFI2D* (Bohlen 2002), which is accurate to $8^{th}$ order spatially, and $2^{nd}$ order temporally. A 2-D model of 4500 by 1000 grid-points is defined, discretised spatially at a 5 m interval, giving a model that is laterally 22.5 km long and by 5 km deep. This spatial discretisation limits the thinnest sill that may be modelled to 5 m. An absorbing perfectly matched layer (PML) boundary of 20 grid-points is included on all sides of the model, with no free surface, which eliminates any sea-surface multiples and ghosts and reduces unwanted

reflections associated with a finite model domain. Whilst 160 shots were simulated at 100 m intervals, within this paper only two are shown (analysis of processing into final migrated data is left for further research). A single shot takes 20 minutes to compute on 50 CPU processors. A Ricker wavelet with a peak frequency of 14 Hz is used as a point source located at 10 m depth. This represents a typical dominant frequency seen on seismic data at the intruded depths (approximately 5 km) within the Faroe-Shetland Basin (Schofield *et al.* 2015). This gives a dominant wavelength of approximately 140-280 m in the sedimentary succession which is significantly longer then the thickness of the stochastically generated sills. A temporal discretisation of 0.1 ms is used to progress the wavefield for 40,000 time steps, to give a total recording length of 4 s.

## 3. Results

'Snapshots' of modelled seismic wavefield at discrete time steps for two shot locations, one above the sill complex and one at its edge, are analysed to provide a visual understanding of the interaction between the seismic wavefield and the sill complex. By taking the divergence and curl of the modelled wave particle velocities from the finite difference simulation, the P- and S-wavefield can be viewed separately (Dougherty & Stephen 1988). Whilst S-wave energy is not created by the acoustic source in the water column, P-wave to S-wave conversion occurs at the boundaries between fluid-solid (e.g. seabed) or solid-solid (e.g. sediment-sill) layers. Converted waves are known to be strongest where there is a high impedance contrast between layers (such as at a sill boundary).

Figure 2 shows snapshots of seismic wave propagation at four discrete simulation times (0.80, 1.30, 1.80, 2.30 s) from a shot located over the thickest section of the sill complex (Shot 1 -

Figure 1). After 0.80 s, observing the P-wavefield only (Figure 2a-i), there is a high amplitude strong P-wave reflection from the top of the sill complex. The first arriving wave within the water column is the direct 'water wave'. Looking at the S-wavefield (Figure 2a-ii), S-wave energy in the subsurface has been generated at the seabed and sills due to the conversion from P-waves. By 1.30 s, the P-wave has propagated through the sill complex (Figure 2b-i). There is high energy loss of the P-wave through the sills, indicated by a low amplitude of the sub-sill transmitted wavefront. This is due to attenuation of this leading wavefront by scattering of energy by the high impedance sill complex. This is manifested as strong internal multiples generated by the wavefield reverberating within the sill complex, which degrades the overall signal and arrives together with the primary reflections from the sills. Additionally, refractions within the sills, which are leaky guided waves result in an almost complete energy loss of the refracted wavefront beyond the critical angle (indicated by the black dashed line). This is due to leaky waves being characterised by a rapid amplitude loss with distance, compared to the sediment diving wave, for example, which does not not exhibit the same energy loss. At the sills, both reflected and refracted P-waves convert to S-waves. The high amplitudes of the converted waves highlight the strong energy loss to converted waves (Figure 2b-ii). The strongest amplitude converted waves occur at the uppermost sills in the complex where the point-spreading of the input wavefront is at its least and the primary energy has not been attenuated by scattering. By 1.80 s, there is a reflection from the sub-sill target reflector, its low amplitude is due to the lack of energy penetration through the sill complex (Figure 2c-i). Some of the up-going S-wave energy arising from seabed conversion reflected from the sill boundaries and conversions within the sill complex is converted back to P-wave and is recorded on the hydrophones (Figure 2c-ii). However, much of the S-wave energy remains trapped within the subsurface. Finally, by 2.30 s, the energy within the water layer is

dominated by sill converted waves(Figure 2d-i) having propagated within the subsurface at the slower S-wave velocity (Figure 2d-ii).

Figure 3 shows snapshots of the seismic wave propagation at the same four discrete simulation times (0.80, 1.30, 1.80, 2.30 s) for a shot away from the edge of the thick sill complex (Shot 2 - Figure 1), above a number of thinner sills. By 0.80 s, primary reflections from the thin sills are visible. These have a significantly lower amplitude than occurred at thicker sills (Figure 2a-i), but in the absence of noise in this model, they are still detectable. Rather than forming a discrete reflection from a single sill, they represent a reflection from a combination of thin sills. P-S conversions at the seabed and thin sill boundaries also occur (Figure 3a-ii). By 1.30 s, the primary transmitted wavefront has passed through the sill complex to the sub-sill target reflector (Figure 3b-i). In comparison with Figure 2b-i the amplitude is stronger. Where the wavefront reaches the thicker sills, it propagates as leaky guided waves, where eventually the energy decays. In-between the thick sills, waves are guided between the higher velocity sills within the lower velocity sediments. These guided waves are trapped but may lose energy by tunneling through the thin sills and so do not exhibit the same energy loss with distance as the guided waves. Their propagation velocity is determined by the background velocity so they are observed as part of the sediment diving wave. Similarity, leaky converted waves propagate within each thick sill, and the seabed converted energy reflects from the thin sills (Figure 3b-ii). By 1.80 s, a reflection from the target reflector retains the stronger amplitude (Figure 3c-i) than seen for shot 1(Figure 2c-i). There is also a weak P-S conversion from the target reflector below the sill complex (Figure 3c-ii). Finally, by 2.30 s, a high amplitude converted wave, which has eventually converted back to a P-wave at the seabed, is present within the water column (Figure 3d-i). Significant converted energy, mostly from the thin sills, is scattered into the subsurface, and lost (Figure 3d-ii). The transmitted S-wave energy through

the sill complex is too attenuated by the time it reaches the sub sill target so does not provide additional illumination for this target.

Modelled shot gathers for each simulation discussed here shows the response that would be observed on a 6 km towed hydrophone array, to the left hand side of the shot (Figure 4). The lack of reflection from the target below the sill complex is clear where the shot is located directly above the thick sill complex (Figure 4a) compared to away from the complex (Figure 4b). Individual reflections from each sill are a challenge to identify, however for shot 2 in Figure 4b, reflections from the thin sills are observed. Strong converted waves from the sills arrive at the hydrophones beyond 1.5 km offset from the source. These have a higher amplitude than pure P waves arrivals beyond the critical angle (approximately 30 degrees) as demonstrated by a simple 2 layer Zoeppritz model of a plane wave arriving at a sediment-sill boundary (Figure 4c).

## 4. Discussion

These simulations highlight the fundamental challenges faced during seismic exploration in sedimentary basins containing pervasive igneous sill complexes. This is due to seismic wavefield effects that are the dominant causes of reduced imaging. These include: (1) stratigraphic filtering and multiples; (2) converted waves; (3) leaky guided waves; and (4) sub-resolution thin sills.

(1) Stratigraphic filtering and multiples: the most significant example of reduced imaging is over the thickest portion of the sequence (Figure 2). Thick intrusions may mask deeper intrusions due to stratigraphic filtering effects (Deng 1994). At normal incidence, the high

acoustic impedance contrast between the sills and the sediments at the top of the sill complex results in a reflection coefficient of about 0.4 (and therefore a transmission coefficient of 0.6) at a single sediment/sill boundary (Figure 4c), corresponding to a 16% reduction of energy at each sill interface through a stack of sills. However this energy loss is enhanced at each subsequent interface encountered by the wavefront. This also generates a coda of multiple reflections generated within the stack of sills. This creates a challenge when processing these data as these may appear to be part of the primary wavefield and ideally they need to be suppressed to enable a robust interpretation. Whilst there are many sophisticated techniques available to remove multiples from seismic data, the fact this multiple energy arrives coincident with the primary reflections and do not have a predictable periodicity mays them difficult to suppress using statistically based deconvolution methods. Therefore, it is likely that some degradation of the seismic image can be expected due to these multiples. This was observed by Hardy et al. (2008), who suggested that internal multiples that have not been sufficiently removed during processing may give the appearance of sills that are not actually present. However, advances in seismic imaging, such as the Marchenko method which uses multiple energy in generating a seismic image, may be able to take advantage of this (Lomas & Curtis 2019).

(2) Converted waves: for high-impedance contrast media such as sills, the use of elastic modelling as opposed to acoustic is crucial to capture the influence of strong converted modes. These converted modes were missed during the study by Hardy et al. (2008). This study shows that some of the S-wave energy is converted back to P-wave at the seabed, and shows up as high amplitude converted modes on the seismogram. Otherwise, if it remains as S-wave energy within the subsurface, this represents lost energy from the overall wavefield that contributes to degraded imaging. It is often suggested that the converted modes may be used to aid imaging (Jones 2013), however given the lack of

converted mode energy that returns to the surface from the deepest parts of the thick-sill sequence or the target reflector (Figure 2d-ii), caution must be exercised to fully understand the origin of the conversions.

(3) Leaky guided waves: the propagation of the sub-horizontal refracted energy within each individual sill in the form of guided waves. Energy propagating within the sills leaks out, resulting in an overall amplitude decay with distance. Waveguiding effects are observed in many situations, such as leaky waves in gas hydrate layers (Zanoth *et al.* 2007), but have not been reported for sill complexes. Given the rapid attenuation of the leaky guided waves, it is unlikely that use of these would improve imaging. As much of the energy arrives outside of the direct water wave, it is likely that most of this would be muted during seismic processing, although care must be taken to ensure no guided refracted energy around the critical offset is included within reflection processing workflows. Energy trapped and propagating in-between sills within the sediments as intra-sill guided waves are unlikely to form an important contribution to the reflected wavefield, as this energy may only be returned to the surface at very long offsets and because it propagates at the background velocity, it is part of the refracted wavefield.

(4) Sub-resolution thin sills: The modelling performed here suggests that in the absence of noise, reflections from thin sills are observable at low frequency (14 Hz). However, as they have a low amplitude, the arrivals are likely to be unobservable in the presence of ambient noise assoicated with the collection of seismic reflection data.Where mulitple thin sills are present then stronger reflections maybe created by constructive interference so a reflection maybe wrongly interpreted as a being from a single sill or interfaces in a sedimentary succession as was the case in 164/07-1 (Archer et al., 2005). Full-waveform inversion (FWI) has the potential to resolve fine-scale features such as thin sills (Morgan *et al.* 2013).

The model presented here may be considered as a starting point for further research to improve understanding of the interaction of seismic energy with sill complexes, such as including an extrusive basalt overburden (as is common in the Faroe-Shetland Basin), creating more interconnectivity between the sills by including feeder dykes and extension into a 3D modelling study. Though the results within this study focused on the wave propagation effects, further work should include analysis of the final processed image of all the shots by undertaking full processing of synthetic data and making direct comparisons to real seismic datasets. As part of this processing it may prove possible to test strategies that could improve the final image that reduces the risk of misinterpretation. Another possible development would be to integrate this type of modelling into the workflow where seismic interpretation of sill complexes is used to understand subsurface magma transport from a volcanological and/or hydrocarbon point of view (e.g. Schofield et al. 2015; Jackson *et al.* 2020, Walker et al. 2020, Phillips & Magee 2020). However,it should be recognised that there are challenges with imaging sills. In particular, it is probable that not all sills are imaged from deeper within the complex or the multiply scattered wavefield has become too complex to be confident about its interpretation.

## 5. Conclusions

By modelling the entire seismic wavefield around a subsurface sill complex, we have highlighted the dominant causes of reduced sub-sill imaging as strong energy attenuation. This occurs due to stratigraphic filtering, the conversion of P-wave energy to S-wave energy, internal multiples and refractions (leaky guided waves) within individual sills in the form of leaky guided waves. There is almost a complete loss of seismic energy penetrating the sill

complex to a sub-sill target reflector, which has significant implications for sub-sill imaging. Thin sills are shown to have an influence on the overall wavefield, particularly in the generation of converted wave energy, and are resolvable at the frequencies observed in these models, however, they may fall within the background noise level on actual seismic reflection data. Further improvements to sub-sill imaging could be achieved through seismic processing, which should be investigated further using both synthetic and real 3D seismic datasets.

## Acknowledgements

This work was undertaken during O.G.S's PhD at Durham University, funded by Eni through the Volcanic Margins Research Consortium (Phase 2). Seismic modelling was performed using the open source SOFI2D (Bohlen 2002) and post-processed using Seismic Un*x (Stockwell & Cohen 2012). Figures were prepared using the open source Generic Mapping Tools (GMT) (Wessel & Smith W. H. F. 1998) and Seismic Un*x. Zoeppritz amplitude coefficients were calculated using the CREWES Matlab toolbox of the University of Calgary. This work made use of the facilities of the Hamilton HPC Service of Durham University.

## References


Airoldi, G. M., Muirhead, J. D., Long, S. M., Zanella, E., & White, J. D. (2016). Flow dynamics in mid-Jurassic dikes and sills of the Ferrar large igneous province and implications for long-distance magma transport. Tectonophysics, 683, 182-199.

Archer, S.G., Bergman, S.C., Iliffe, J., Murphy, C.M. & Thornton, M. (2005) Palaeogene igneous rocks reveal new insights into the geodynamic evolution and petroleum potential of the Rockall Trough, NE Atlantic Margin. *Basin Res.*, **17**, 171–201. doi:10.1111/j.1365-2117.2005.00260.x

Bohlen, T. (2002) Parallel 3-D viscoelastic finite difference seismic modelling. *Comput. Geosci.*, **28**, 887–899.

Brocher, T.M. (2005) Empirical relations between elastic wavespeeds and density in the Earth's crust. *Bull. Seismol. Soc. Am.*, **95**, 2081–2092. doi:10.1785/0120050077

Cartwright, J. & Møller Hansen, D. (2006) Magma transport through the crust via interconnected sill complexes. *Geology*, **34(11)**, 929-932.

Deng, H.L. (1994) Acoustic-wave propagation in thin-layered media with steep reflectors. *Geophysics*, **59**, 1593–1604.

Dougherty, M.E. & Stephen, R.A. (1988) Seismic energy partitioning and scattering in laterally heterogeneous ocean crust. *Pure Appl. Geophys. PAGEOPH*, **128**, 195–229. doi:10.1007/BF01772597

Eide, C.H., Schofield, N., Lecomte, I., Buckley, S.J. & Howell, J.A. (2017) Seismic interpretation of sill complexes in sedimentary basins : implications for the sub-sill imaging problem. *J. Geol. Soc. London*, **175**, 193–209. doi:10.1144/jgs2017-096

Gallagher, J.W. & Dromgoole, P.W. (2007) Exploring below the basalt, offshore Faroes: a case history of sub-basalt imaging. *Pet. Geosci.*, **13**, 213–225. doi:10.1144/1354-079306-711

Goff, J.A., Holliger, K. & Levander, A.R. (1994) Modal fields: A new method for characterisation of random seismic velocity heterogeneity. *Geophys. Res. Lett.*, **21**, 493–496.

Goff, J.A. & Levander, A.R. (1996) Incorporating "sinuous connectivity" into stochastic models of crustal heterogeneity: Examples from the Lewisian gneiss complex, Scotland, the Franciscan formation, California, and the Hafafit Gneiss Complex, Egypt. *J. Geophys. Res. Solid Earth*, **101**, 8489–8501. doi:10.1029/96JB00110

Hardy, R.J., Bednar, J.B., Bednar, C., Fernandes, K. & Jones, S.M. (2008) Imaging Beneath Igneous Sills Using Reverse Time Depth Migration. *EAGE Expand. Abstr. 2008*.

Jackson, C.A.L., Magee, C. & Jacquemyn, C. (2020) Rift-related magmatism influences petroleum systems development in the NE Irish Rockall Basin, offshore Ireland. *Pet. Geosci.*

Jones, I.F. (2013) Tutorial: The seismic response to strong vertical velocity change. *First Break*, **31**, 79–90. doi:10.3997/1365-2397.2013018

Larkin, S.P., Levander, A.R., Okaya, D. & Goff, J.A. (1996) A deterministic and stochastic velocity model for the Salton Trough/Basin and Range transition zone and constraints on magmatism during rifting. *J. Geophys. Res.*, **101**, 27883–27. doi:199610.1029/96JB02535

Lecomte, I., Lavadera, P.L., Botter, C., Anell, I., Buckley, S.J., Eide, C.H., Grippa, A., *et al.* (2016) 2(3)D convolution modelling of complex geological targets beyond – 1D convolution. *First Break*, **34**, 99–107. Retrieved from http://fb.eage.org/publication/content?id=84451

Levander, A.R., England, R.W., Smith, S.K., Hobbs, R.W., Goff, J.A. & Holliger, K. (1994) Stochastic characterization and seismic response of upper and middle crustal rocks based on the Lewisian gneiss complex, Scotland. *Geophys. J. Int.*, **119**, 243–259. doi:10.1111/j.1365-246X.1994.tb00925.x

Lomas, A. & Curtis, A. (2019) An introduction to Marchenko methods for imaging. *Geophysics*,

**84**, F35–F45. doi:10.1190/geo2018-0068.1

Magee, C., Maharaj, S.M., Wrona, T. & Jackson, C.A.L. (2015) Controls on the expression of igneous intrusions in seismic reflection data. *Geosphere*, **11**, 1024–1041. doi:10.1130/GES01150.1

Magee, Craig, James D. Muirhead, Alex Karvelas, Simon P. Holford, Christopher AL Jackson, Ian D. Bastow, Nick Schofield et al. "Lateral magma flow in mafic sill complexes." Geosphere 12, no. 3 (2016): 809-841.

Maresh, J., White, R.S., Hobbs, R.W. & Smallwood, J.R. (2006) Seismic attenuation of Atlantic margin basalts: Observations and modeling. *Geophysics*, **71**, B211–B221. doi:10.1190/1.2335875 Downloaded

Mark, N.J., Holford, S., Schofield, N., Eide, C.H., Pugliese, S., Watson, D. & Muirhead, D. (2019) Structural and lithological controls on the architecture of igneous intrusions: examples from the NW Australian Shelf. *Pet. Geosci.*

Mark, N.J., Schofield, N., Pugliese, S., Watson, D., Holford, S., Muirhead, D., Brown, R.J., *et al.* (2017) Igneous intrusions in the Faroe Shetland basin and their implications for hydrocarbon exploration; new insights from well and seismic data. *Mar. Pet. Geol.* doi:10.1016/j.marpetgeo.2017.12.005

Martini, F. & Bean, C.J. (2002) Interface scattering versus body scattering in subbasalt imaging and application of prestack wave equation datuming. *Geophysics*, **67**, 1593–1601. doi:10.1190/1.1512750

Morgan, J., Warner, M., Bell, R., Ashley, J., Barnes, D., Little, R., Roele, K., *et al.* (2013) Next-generation seismic experiments: Wide-angle, multi-azimuth, three-dimensional, full-waveform inversion. *Geophys. J. Int.*, **195**, 1657–1678. doi:10.1093/gji/ggt345

Muirhead, J.D., Airoldi, G., Rowland, J.V. and White, J.D. (2012) Interconnected sills and inclined sheet intrusions control shallow magma transport in the Ferrar large igneous

province, Antarctica. *Bulletin*, *124*(1-2), pp.162-180.

Phillips, T. & Magee, C. (2020) Structural controls on the location, geometry, and longevity of an intraplate volcanic system - The Tuatara Volcanic Field, Great South Basin, New Zealand. *J. Geol. Soc. London*. doi:10.31223/osf.io/b94ds

Rabbel, O., Galland, O., Mair, K., Lecomte, I., Senger, K., Spacapan, J.B. & Manceda, R. (2018) From field analogues to realistic seismic modelling : a case study of an oil-producing andesitic sill complex in the Neuquén Basin , Argentina.

Rateau, R., Schofield, N. & Smith. (2013) The potential role of igneous intrusions on hydrocarbon migration, West of Shetland. *Petroleum Geoscience*, ***19***(3), pp.259-272.

Schofield, N., Holford, S.P., Millett, J.M., Brown, D.J., Jolley, D., Passey, S.R., Muirhead, D., *et al.* (2015) Regional magma plumbing and emplacement mechanisms of the Faroe-Shetland Sill Complex: Implications for magma transport and petroleum systems within sedimentary basins. *Basin Res.*, 1–23.

Schofield, N.J., Brown, D.J., Magee, C. and Stevenson, C.T. (2012) Sill morphology and comparison of brittle and non-brittle emplacement mechanisms. *Journal of the Geological Society*, **169(2)**, 127-141.

Smallwood, J.R. & Maresh, J. (2002) The properties, morphology and distribution of igneous sills: modelling, borehole data and 3D seismic from the Faroe-Shetland area. *Geol. Soc. London, Spec. Publ.*, **197**, 271–306.

Stockwell, J.W. & Cohen, J.K. (2012) CWP/SU: Seismic Un*x Release No.43r3: an open source software package for seismic research and processing, Center for Wave Phenomena, Colorado School of Mines.

Thomson, K. & Hutton, D. (2004) Geometry and growth of sill complexes: insights using 3D seismic from the North Rockall Trough. *Bull. Volcanol.*, **66**, 364–375. doi:10.1007/s00445-003-0320-z

Walker, R., Stephens, T., Greenfield, C., Gill, S., Healy, D. and Poppe, S. (2020) Segment tip geometry of sheet intrusions, I: Theory and numerical models for the role of tip shape in controlling propagation pathways, *Volcanica, 4*(2),189-201.

Wessel, P. & Smith W. H. F. (1998) New, improved version of the Generic Mapping Tools released, EOS Trans. AGU, 79, 579.

Wright, T.J., Sigmundsson, F., Pagli, C., Belachew, M., Hamling, I.J., Brandsdóttir, B., Keir, D., Pedersen, R., Ayele, A., Ebinger, C. & Einarsson, P. (2012) Geophysical constraints on the dynamics of spreading centres from rifting episodes on land., *Nature Geoscience,* 5(4)

Zanoth, S.R., Saenger, E.H., Krüger, O.S. & Shapiro, S.A. (2007) Leaky mode: A mechanism of horizontal seismic attenuation in a gas-hydrate-bearing sediment. *Geophysics*, **72**, E159. doi:10.1190/1.2750375

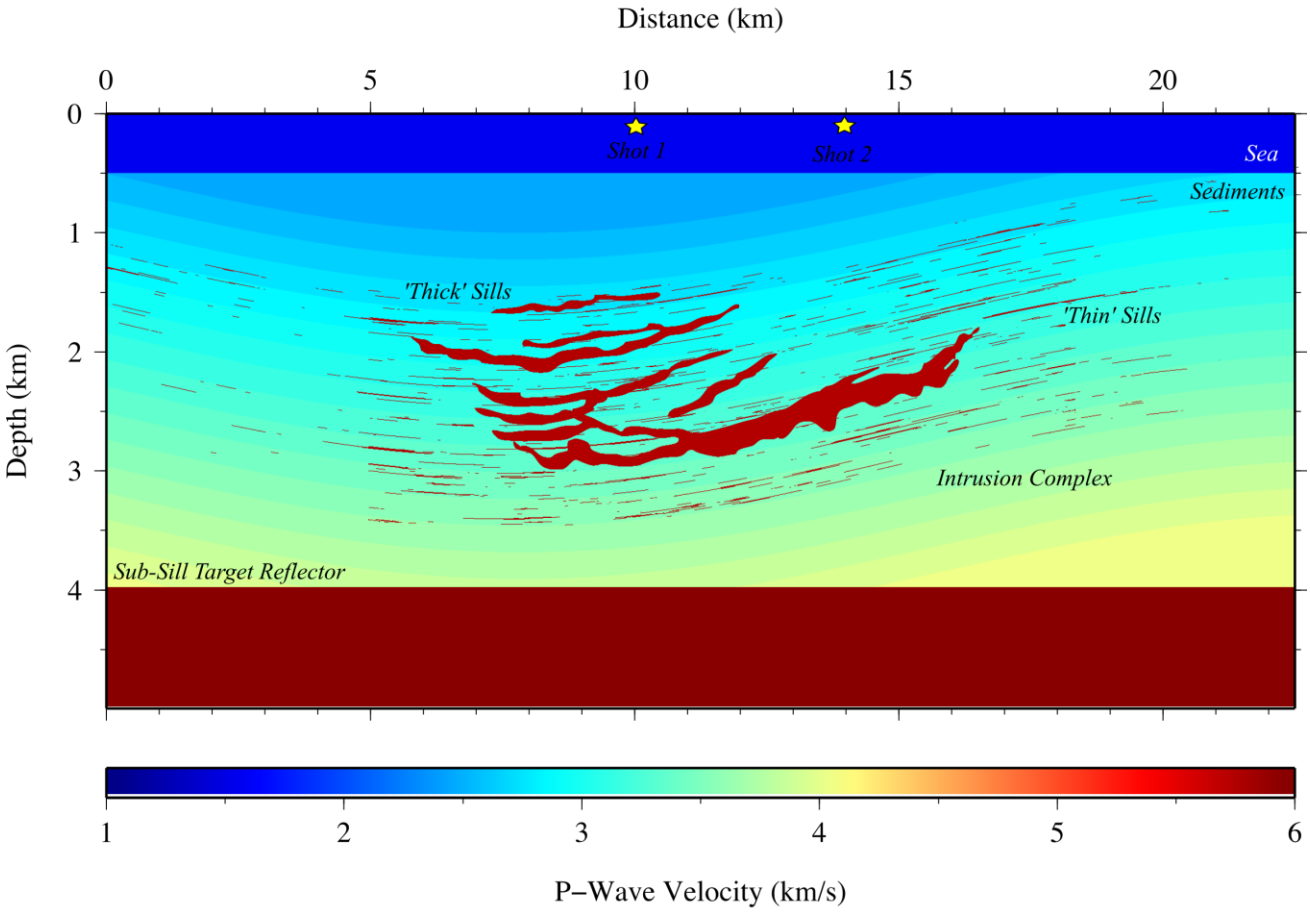


*Figure 1: P-wave velocity model containing both seismically resolvable 'thick' sills taken from the interpreted seismic data, and unresolvable 'thin' sills. Two shot locations are presented here, 'Shot 1' at 10 km and 'Shot 2' at 14 km.*

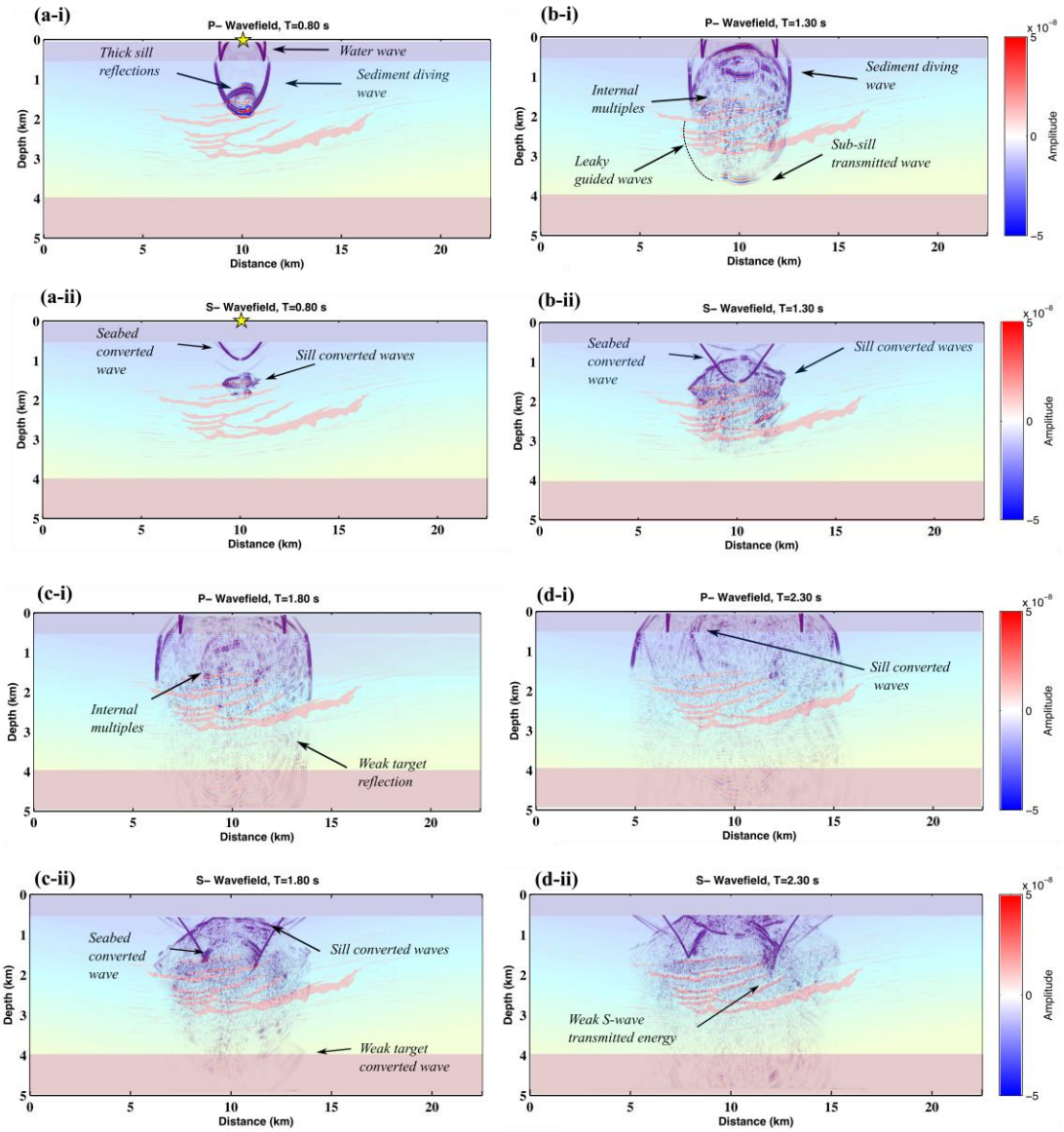


*Figure 2: Snapshots of seismic wave propagation for 'Shot 1' (yellow star) after 0.80 (a), 1.30 (b), 1.80 (c) and 2.30 (d) seconds for the P- (i) and S- (ii) wavefield.*

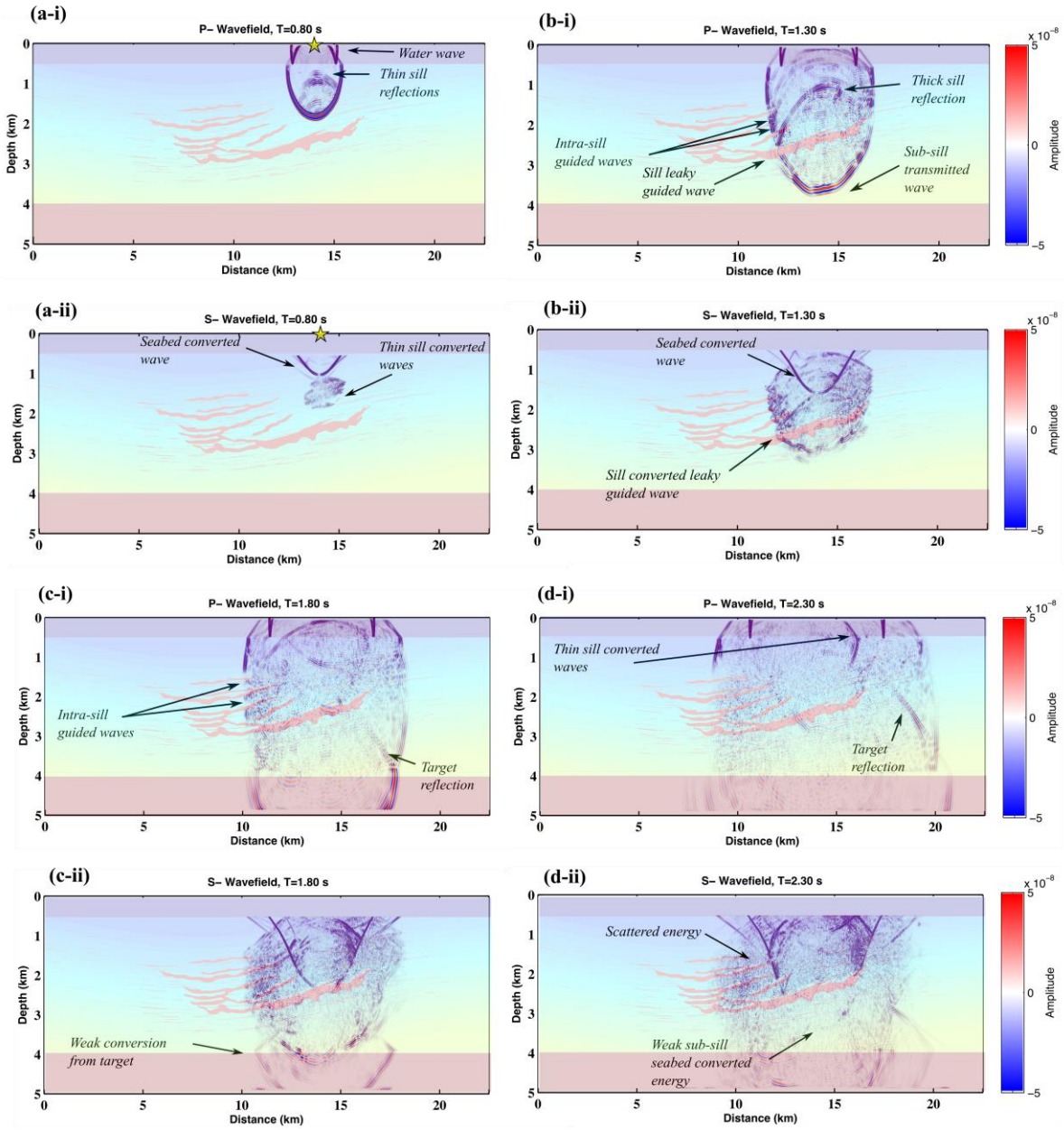


*Figure 3: Snapshots of seismic wave propagation for 'Shot 2' (yellow star) after 0.80 (a), 1.30 (b), 1.80 (c) and 2.30 (d) seconds for the P- (i) and S- (ii) wavefield.*

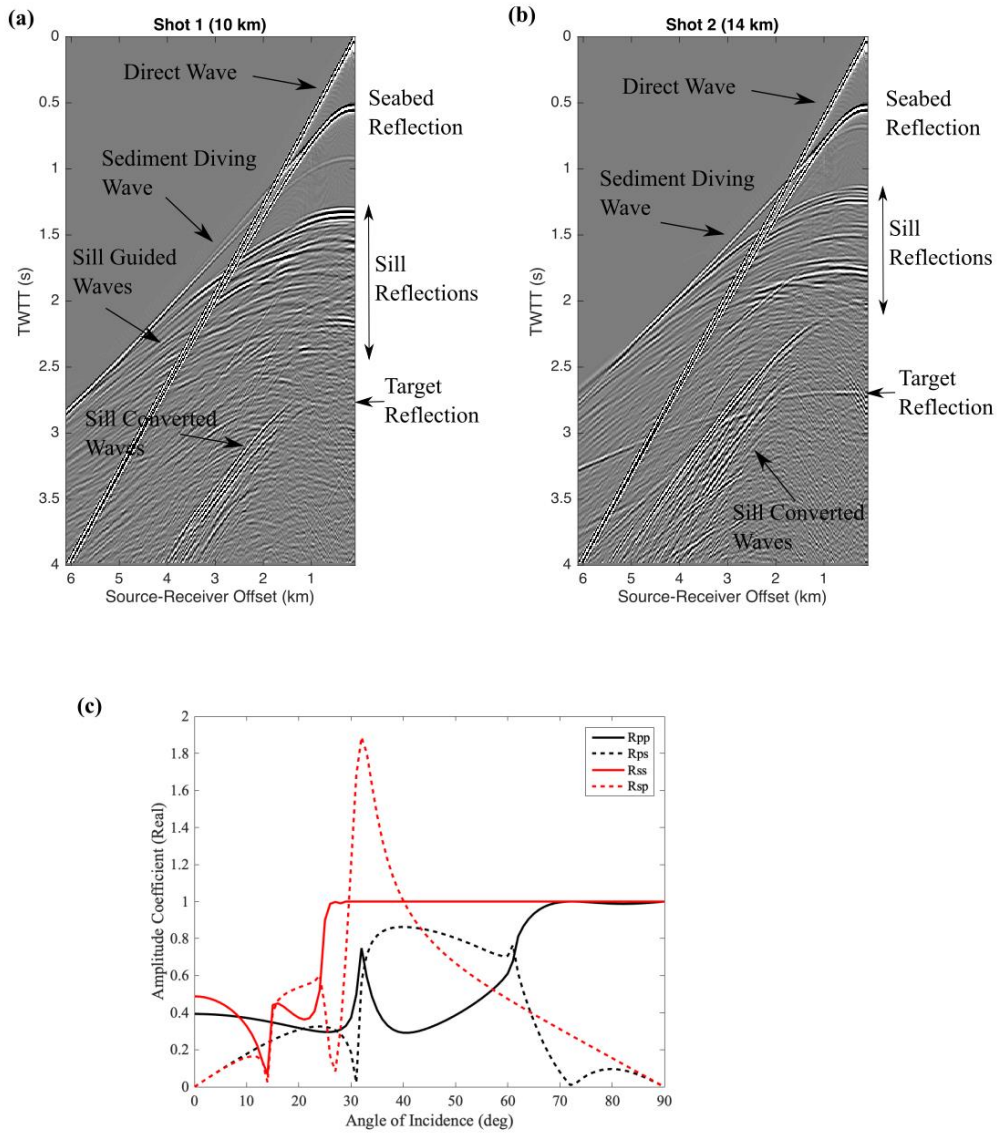


*Figure 4: Simulated shot gathers for (a) Shot 1 at 10 km and (b) Shot 2 at 14 km. (c) Zoeppritz reflection coefficients for an incident P-wave (black) and S-wave (red) at a sediment/intrusion boundary, plotted against angle of incidence. Sediment: $V_p$=3 km/s, $V_s$=1.4 km/s, rho=2.2 kg/m$^3$. Intrusion: $V_p$=5.75 km/s, $V_s$=3.4 km/s, rho=2.7 kg/m$^3$. Rpp = reflected P-wave, Rss = reflected S-wave. Reflected converted phases (Rps = P-wave to S-wave, Rsp = S-wave to P-wave) are shown by dashed lines.*